MITP/16-074
HIM-2016-03

$B_s\pi^+$ scattering and search for $X(5568)$ with lattice QCD

C. B. Lang,[1,*] Daniel Mohler,[2,3,†] and Sasa Prelovsek[4,5,‡]

[1] *Institute of Physics, University of Graz, A–8010 Graz, Austria*
[2] *Helmholtz-Institut Mainz, 55099 Mainz, Germany*
[3] *Johannes Gutenberg Universitat Mainz, 55099 Mainz, Germany*
[4] *Department of Physics, University of Ljubljana, 1000 Ljubljana, Slovenia*
[5] *Jozef Stefan Institute, 1000 Ljubljana, Slovenia*

(Dated: October 12, 2016)

We investigate $B_s\pi^+$ scattering in s-wave using lattice QCD in order to search for an exotic resonance $X(5568)$ with flavor $\bar{b}s\bar{d}u$; such a state was recently reported by D0 but was not seen by LHCb. If $X(5568)$ with $J^P = 0^+$ exists, it can strongly decay only to $B_s\pi^+$ and lies significantly below all other thresholds, which makes a lattice search for $X(5568)$ cleaner and simpler than for other exotic candidates. Both an elastic resonance in $B_s\pi^+$ as well as a deeply bound $B^+\bar{K}^0$ would lead to distinct signatures in the energies of lattice eigenstates, which are not seen in our simulation. We therefore do not find a candidate for $X(5568)$ with $J^P = 0^+$ in agreement with the recent LHCb result. The extracted $B_s\pi^+$ scattering length is compatible with zero within the error.

arXiv:1607.03185v2 [hep-lat] 11 Oct 2016

I. INTRODUCTION

The D0 collaboration reported evidence for a relatively narrow peak in the $B_s\pi^+$ invariant mass not far above threshold [1]. The peak was attributed to a resonance $X(5568)$ with mass $m_X = 5567.8 \pm 2.9^{+0.9}_{-1.9}$ MeV and width $\Gamma_X = 21.9 \pm 6.4^{+5.0}_{-2.5}$ MeV with significance 5.1 σ, while its quantum numbers were not measured. Its decay to $B_s\pi^+$ implies exotic flavor structure $\bar{b}s\bar{d}u$. The LHCb collaboration subsequently investigated the cross-section as a function of the $B_s\pi^+$ invariant mass with increased statistics and did not find any peak in the same region [2].

If the state $X(5568)$ with flavor $\bar{b}s\bar{d}u$ and some J^P exists, it is unique among exotic candidates, as it can strongly decay only in one final state $B_s\pi^+$ and is relatively far below other thresholds. This allows for a more reliable, cleaner and simpler theoretical search for it within QCD, which will be elaborated below. Most notably, the next threshold for most J^P choices is $B^+\bar{K}^0$, which lies about 210 MeV above $X(5568)$ and is therefore not expected to play a notable role for this state. The only nearby threshold is $B_s^*\pi^+$, which lies within the width of $X(5568)$ and it couples to this state only if its quantum numbers are $J^P = 1^-$.

Most theoretical studies which accommodate a $X(5568)$ propose $J^P = 0^+$. A number of QCD sum-rule studies do find $X(5568)$ (for example [3–5]), but these assume that a continuum of scattering states starts above the isolated $X(5568)$ pole, which is a questionable approach for a resonance. Reference [6] finds $X(5568)$ as a $B^+\bar{K}^0$ bound state, while all other works [7–10] disfavor this option in view of the large binding energy $\simeq 210$ MeV. A state is also found within the tetraquark models [11, 12] and quark models [13], while other quark model studies [14, 15] do not confirm it. The approaches based on Hybridized Tetraquarks [16] and Unitarized Effective field theory [17, 18] do not favour its existence. A number of physics scenarios were considered in [9, 10], all disfavouring the $X(5568)$.

In this paper we present the first study of $B_s\pi^+$ and $B^+\bar{K}^0$ scattering within lattice QCD in order to search for the $X(5568)$. We consider the channel $J^P = 0^+$ where $B_s\pi^+$ and $B^+\bar{K}^0$ are in s-wave, which is favoured by several phenomenological studies (for example [3, 6, 11–13]). The major simplification in the ab-initio lattice search for $X(5568)$ comes from the fact that it can strongly decay only to $B_s\pi^+$, while the next relevant threshold $B^+\bar{K}^0$ is significantly higher. The task is therefore to study elastic $B_s\pi^+$ scattering. During the last decade, the lattice community has successfully demonstrated the extraction of hadronic resonances that appear in elastic scattering (see for example [19–23]) by determining the scattering matrix using the so-called Lüscher formalism [24, 25]. We apply the same well-established formalism to determine whether $B_s\pi^+$ scattering has a resonant or non-resonant shape. For completeness, we consider both channels $B_s\pi^+$ and $B^+\bar{K}^0$ coupled together, which should render a lattice signature for $X(5568)$ even if it was predominantly a deeply bound $B^+\bar{K}^0$ state. Note that $B_s\pi^+$ scattering is elastic in the wide region below $B^+\bar{K}^0$, and there the well-tested formalism is reliable.

Section II provides an analytic prediction for the energies of lattice eigenstates in case an $X(5568)$ claimed by D0 existed. The technical details of simulation and analysis are elaborated in Section III. The eigenenergies from the actual simulation are presented in Section IV, where a comparison to the analytic prediction is made. We conclude that the results from the simulation do not support the existence of $X(5568)$ with $J^P = 0^+$.

* christian.lang@uni-graz.at
† mohler@kph.uni-mainz.de
‡ sasa.prelovsek@ijs.si

II. EXPECTED SIGNATURES OF $X(5568)$

The lattice simulation determines the energies of QCD eigenstates with given quantum numbers for finite spatial size L. We consider the quantum numbers $J^P = 0^+$, the flavor content $\bar{b}s\bar{d}u$, total momentum zero, while the spatial size of our lattice is $L \simeq 2.9$ fm. Before presenting the energies obtained from the simulation, we illustrate what would be the distinct features in the spectrum if $X(5568)$ exists. We will argue that an eigenstate with energy $E \simeq m_X$ is expected in a scenario with $X(5568)$, while there is no such eigenstate in absence of $X(5568)$.

A. Resonance in $B_s\pi^+$

The $X(5568)$ appears as a peak in the $B_s\pi^+$ invariant mass and is naturally considered as an elastic resonance in $B_s\pi^+$, whatever the origin of this exotic state may be. The hypothesis with and without a resonance lead to very distinct spectra of eigenenergies, as shown by solid and dashed lines in Figure 1. In case B_s and π^+ do not interact, they have back-to-back momenta $\mathbf{p} = 2\pi\mathbf{n}/L$ due to the periodic boundary conditions in space, and the energies of $B_s(n)\pi^+(-n)$ eigenstates (momenta in units of $2\pi/L$ are given in parentheses)

$$E^{n.i.}(L) = \sqrt{m_{B_s}^2 + \left(\frac{2\pi\mathbf{n}}{L}\right)^2} + \sqrt{m_\pi^2 + \left(\frac{2\pi\mathbf{n}}{L}\right)^2}, \quad \mathbf{n} \in N^3 \tag{1}$$

are represented by the dashed orange lines. The red solid lines represent the expected energies of the $B_s\pi^+$ system in case of a resonance $X(5568)$. They result from the resonant Breit-Wigner-type phase shift

$$\delta_{B_s\pi}(p) = \text{atan}\left[\frac{E\,\Gamma(E)}{m_X^2 - E^2}\right], \quad \Gamma(E) = \Gamma_X \frac{p(E)m_X^2}{p(m_X)E^2}, \tag{2}$$

where m_X and Γ_X are the observed mass and width of $X(5568)$ [1]. The (infinite-volume) elastic phase shift $\delta(E)$ and the discrete energies of eigenstates E on the lattice of size L are related via the rigorous Lüscher's relation [24, 25]

$$\delta_{B_s\pi}(p) = \text{atan}\left[\frac{\sqrt{\pi}pL}{2\,Z_{00}(1;(pL/2\pi)^2)}\right] \tag{3}$$
$$\text{where } E(p) = \sqrt{m_{B_s}^2 + p^2} + \sqrt{m_\pi^2 + p^2}\,.$$

The eigen-energies E in the scenario with $X(5568)$ are obtained by inserting the resonant phase shift (2) to the left-hand-side of (3) and solving for discrete p, which gives E. The resulting discrete eigen-energies $E(L)$ are shown for a range of L by the red curves in Figure 1. The resonant scenario predicts an eigenstate near $E \simeq m_X$ (red solid), while there is no such eigenstate for $L = 2-4$ fm in a scenario with no or small interaction between B_s and π^+ (orange dashed). These are distinct and robust features in the spectra, which do not get modified for different parametrisations in the resonant scenario, or for different interaction in the non-resonant scenario.

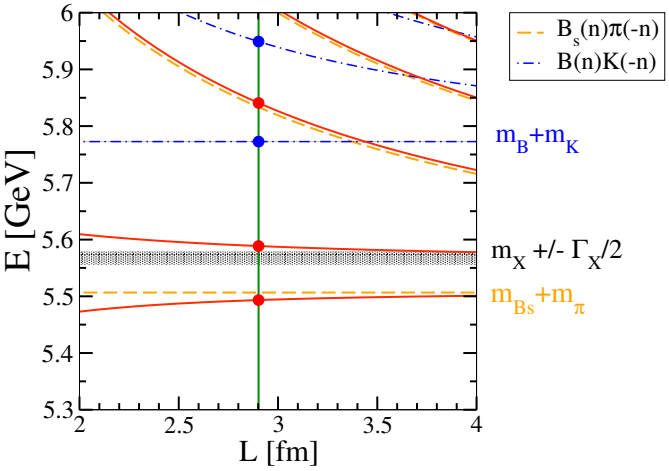

FIG. 1. Analytic predictions for energies $E(L)$ of eigenstates as a function of lattice size L: red solid lines are $B_s\pi$ eigenstates in the scenario with resonance $X(5568)$ [1]; orange dashed lines are $B_s\pi$ eigenstates when B_s and π do not interact; blue dot-dashed lines are $B^+\bar{K}^0$ eigenstates when B^+ and $\bar{K}^0$ do not interact; the grey band indicates the position of $X(5568)$ from the D0 experiment [1]. Physical masses of hadrons are used. The lattice size $L = 2.9$ fm, that is used in our simulation, is marked by the vertical line.

At and above the $B^+\bar{K}^0$ threshold, these states also appear as eigenstates and will be considered in our simulation. For our lattice parameters $X(5568)$ is far below $B^+\bar{K}^0$ threshold and one would not expect a strong influence from that channel unless the dynamics leads to a really strong coupling. The dot-dashed blue lines show the energies of non-interacting $B^+(n)\bar{K}^0(-n)$ in the limit when both channels are decoupled.

B. Deeply bound $B^+\bar{K}^0$

Next we consider the unlikely scenario where the $X(5568)$ is a very deeply bound $B^+\bar{K}^0$ state, in the limit where it is decoupled from $B_s\pi^+$. Then a simulation would render an eigenstate with $E \simeq m_X$ up to exponentially small correction in L, with $\lim_{L\to\infty} E(L) = m_X$. In addition there would be almost non-interacting states $B_s(n)\pi^+(-n)$ and $B^+(n)\bar{K}^0(-n)$ near orange and blue lines, respectively. For the simulated $L \simeq 2.9$ fm, the number of eigenstates is therefore the same as for the resonant scenario. The values of expected energies are also similar, up to the small energy shifts. This remains true in a scenario with a deeply bound $B^+\bar{K}^0$ state which also couples to $B_s\pi^+$.

III. LATTICE SIMULATION DETAILS

A. Gauge configurations

We employ gauge configurations from the PACS-CS collaboration, with $N_f = 2+1$ dynamical quarks, lattice spacing $a = 0.0907(13)$ fm, $V = 32^3 \times 64$, $L \simeq 2.9$ fm and $m_\pi = 156(7)(2)$ MeV [26]. Our own fit for the pion mass yields a somewhat larger value of 162.6(2.2)(2.3)MeV. The light and strange quarks are non-perturbatively improved Wilson fermions.

Closer inspection of that ensemble shows that there are a few configurations responsible for a strong fluctuation of the pion mass. In our analysis we consider both the full set of gauge configurations and a subset where four configurations [1] leading to strong fluctuations in the pion mass are removed. This results in a pion mass for the subset roughly 6 MeV larger than quoted above. We demonstrate below that our final conclusions are independent of this choice.

B. Quark mass parameters

For the light up/down quarks the mass parameter of the original simulation is used [26]. For the strange quark we use a partially quenched setup with the valence mass m_s^{val} closer to the physical point than the dynamical sea quark mass m_s^{dyn} [26], leading to $m_K = 504(1)(7)$ MeV [27]. The bottom quark is treated as a valence quark using the Fermilab method [28, 29], where the kinetic masses (M_2) are tuned to experiment and the energy differences are less prone to discretization effects compared to the energies themselves. The bottom quark mass is fixed as discussed in [30] which renders a spin-averaged kinetic mass $\frac{1}{4}(M_2^{B_s} + 3M_2^{B_s^*}) = 5.086(135)(73)$ GeV somewhat smaller than in experiment $E_{\overline{B}_s}^{exp} = \frac{1}{4}(m_{B_s} + 3m_{B_s^*}) = 5.4032(18)$ GeV. The mass splittings of various hadrons containing a b-quark are in good agreement with experiment (see Table II of [30]).

C. Dispersion relations

Here we discuss the dispersion relation between energy, mass and momentum of the pion and B_s. This is needed to determine the s-wave scattering length a_0 for $B_s\pi$ scattering from the ground state lattice energy E_{gr}^{lat} using Lüscher's relation [24, 25]. The momentum p_{gr} is obtained from $E_{gr}^{lat} = E_\pi(p_{gr}) + E_{B_s}(p_{gr})$. For the pion we use the relativistic dispersion relation

$$E_\pi(p) = (m_\pi^{lat} + p^2)^{1/2} \tag{4}$$

and for the heavy meson B_s the Fermilab dispersion relation [28, 29]

$$E_{B_s}(p) = M_1 + p^2/(2M_2) - p^4/(8M_4^3)\ . \tag{5}$$

The values $M_1 = 1.61246(54)$, $M_2 = 2.298(70)$ and $M_4 = 1.59(54)$ have been determined in [30] by measuring $E_{B_s}(p)$ for several small values of p on our lattice. These are the values for the correlated fits with all gauge configurations. When excluding close to exceptional configurations we redo the whole analysis with the reduced set.

Within the Fermilab approach, the rest masses have large discretization effects but mass differences are expected to be close to physical [31] and can be compared to experiment. In order to compare the splitting $E^{lat} - \bar{m}^{lat}$ with $E^{exp} - \bar{m}^{exp}$, we will sometimes plot

$$E = E_n^{lat} - E_{\overline{B}_s}^{lat} + E_{\overline{B}_s}^{exp} \tag{6}$$

where $E_{\overline{B}_s}^{lat}$ is the spin-averaged ground state energy of the B_s system from our simulation and $E_{\overline{B}_s}^{exp}$ is the corresponding physical energy $\frac{1}{4}(m_{B_s} + 3m_{B_s^*})$ from experiment.

D. Lattice operators

To determine the energies of a system with $J^P = 0^+$ and total momentum zero, we employ six interpolating fields[2] of meson-meson type, where each meson is projected to a definite momentum:

$$\begin{aligned} O_{1,2}^{B_s(0)\pi(0)} &= \left[\,\bar{b}\Gamma_{1,2}s\,\right](\mathbf{p}=0)\left[\,\bar{d}\Gamma_{1,2}u\,\right](\mathbf{p}=0) \\ O_{1,2}^{B_s(1)\pi(-1)} &= \sum_{\mathbf{p}=\pm\mathbf{e_{x,y,z}}\ 2\pi/L} \left[\bar{b}\Gamma_{1,2}s\right](\mathbf{p})\left[\bar{d}\Gamma_{1,2}u\right](-\mathbf{p}) \\ O_{1,2}^{B(0)K(0)} &= \left[\,\bar{b}\Gamma_{1,2}u\,\right](\mathbf{p}=0)\left[\,\bar{d}\Gamma_{1,2}s\,\right](\mathbf{p}=0) \end{aligned} \tag{7}$$

with $\Gamma_1 = \gamma_5$ and $\Gamma_2 = \gamma_5\gamma_t$.

One could use also local or quasi-local diquark-antidiquark operators, for example $[\bar{b}C\gamma_5\bar{d}]_{3_c}[sC\gamma_5 u]_{\bar{3}_c}$, but these can be expressed via Fierz transformations as $\sum_i M_1^i(p)M_2^i(-p)$, where $M_1^iM_2^i = B_s\pi, B_s^*\rho, B_{s1}a_1, BK, B^*K^*, B_1K_1, ...$ (see [32] for a detailed discussion).

The $B_s\pi$ and BK are the essential ones for the energy region near $X(5568)$ and are already included in our choice (7). It remains to be seen if structures with significantly separated diquark and antidiquark [33] could be also be probed[3] by meson-meson operators like (7), or if specific implementation of those is needed.

---

[1] The PACS-CS configurations leading to largest fluctionations are hM-001460, jM-000260, jM-000840 and jM-000860.

[2] The interpolators transform according to the A_1^+ irreducible representation of discrete group O_h.

[3] In view of this, we note that the conclusions of our previous studies of X(3872), Y(4140) [32] and Z_c^+ [34] apply to (quasi) local $[qq][\bar{q}\bar{q}]$, but they do not apply to the case of significantly separated $[qq]$ and $[\bar{q}\bar{q}]$.

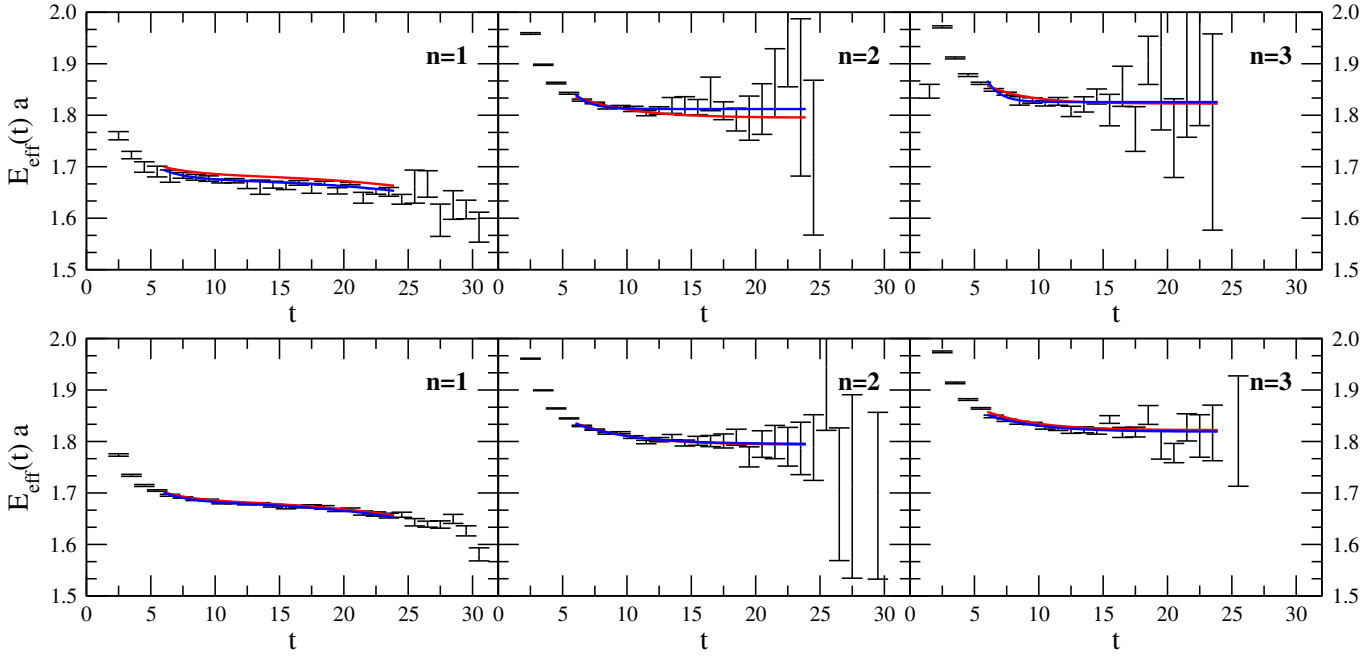

FIG. 2. The effective energies $E_{eff}(t) \equiv \log(\lambda(t)/\lambda(t+1))$ and the curves due to our eigenvalue fits over the fit range $6 \le t \le 24$ for the cases "all,A" (top panes) and "all-4,A" (bottom panes) defined in the caption of Figure 3. From left to right the plots show the ground state, first excited state and second excited state. The fit model (11) was used for the ground state, while the form (10) was employed for the higher states. The correlated (uncorrelated) fits are shown by red (blue) curves.

E. Correlation matrix and eigenenergies

The energies E_n of eigenstates $|n\rangle$ are obtained from the correlation matrix

$$C_{jk}(t) = \langle \Omega | O_j(t'+t) O_k^\dagger(t') | \Omega \rangle = \sum_n Z_j^n Z_k^{n*} \; e^{-E_n t} \tag{8}$$

which also contains the information on the overlaps $Z_j^n \equiv \langle \Omega | \mathcal{O}_j | n \rangle$.

All quark lines run between source and sink, there are no "backtracking" loops. There are only two diagram types: (a) $(B_s \leftrightarrow B_s)(\pi \leftrightarrow \pi)$ and $(B \leftrightarrow B)(K \leftrightarrow K)$ and (b) $B_s\pi \leftrightarrow BK$ where the s and u quarks exchange partners. The Wick contraction gives for (a) a product of two traces, for (b) only one trace.

The correlation matrix elements are calculated using the stochastic distillation method proposed in [35]. In the distillation method [36] the quark fields in the interpolators are smeared according to $q \equiv \sum_{k=1}^{N_v} v^{(k)} v^{(k)\dagger} q_{point}$; in the stochastic version [35] one uses random combination of the sources. We use $N_v = 192$ eigenvectors of the lattice laplacian $v^{(k)}$ reducing them to 16 combinations. The method is convenient for calculating a variety of Wick contractions. The details of our implementaion are presented in [27] where we apply it to D_s states.

Energies E_n and overlaps Z_j^n are extracted from the correlation matrix $C_{jk}(t)$ using the generalized eigenvalue method [37–40]

$$C(t) u^{(n)}(t) = \lambda^{(n)}(t) C(t_0) u^{(n)}(t) \; , \tag{9}$$

where $\lambda^{(n)}(t) \propto e^{-E_n t}$ at large t. Correlated and uncorrelated fits to $\lambda^{(n)}(t)$ are used and $t_0 = 2$.

F. Choice of operator subsets

Although we compute the full 6×6 correlation matrix we attempt to minimize the statistical noise by choosing subsets of most important operators. The guiding principle is the stability of the overlap factors $Z_n^i(t)$ over the fit range and the statistical noise of the eigenvalues. From the overlap factors we identify the dominantly contributing lattice operators to each eigenstate.

G. Energy fits

Ideally the eigenvalues follow a pure exponential behaviour. Due to the limited set of operators there are contaminating contributions from higher excitations at small propagation distances. The finite-time effects (like backward propagation) due to the anti-periodic boundary conditions in time and $n_T = 64$ are important for large distances and even more for light particles. For this reason one chooses a fit model that, in addition to the leading exponential form, allow for such contributions.

For larger energies and propagation distances much less than $n_T/2$ the finite size effects are negligible and we fit $\lambda(t)$ to

$$f(t) = a_1\, \mathrm{e}^{-E_1\, t} + a_2\, \mathrm{e}^{-E_2\, t} \tag{10}$$

ensuring that $E_1 < E_2$. The second term effectively represents possible higher excitation visible at small t values, allowing for a larger fit range. We use this form for eigenstates above the ground state.

For two-meson eigenstates with light particles and long propagation time one has to choose a form that can represent also (a) the propagation back in time, (b) the propagation of one meson in one direction and the second meson in the opposite direction of time (see, e.g., Appendix in [41]). In our study this concerns the $B_s\pi$ ground state and we use

$$\begin{aligned} f(t) = a_1 &\left(\mathrm{e}^{-E_1\, t} + \mathrm{e}^{-E_1\,(n_T-t)}\right) \\ &+a_2 \left(\mathrm{e}^{-E_2\, t} + \mathrm{e}^{-E_2\,(n_T-t)}\right) \\ &+a_3 \left(\mathrm{e}^{-m_\pi t - m_{B_s}(n_T-t)} + \mathrm{e}^{-m_{B_s} t - m_\pi (n_T-t)}\right) \end{aligned} \tag{11}$$

(again checking that $E_1 < E_2$) and where m_π and m_{B_s} have been determined from the corresponding single-meson correlators (see Subsection III C).

Figure 2 gives an example of these fits showing the effective energies $E_{eff}(t) \equiv \log(\lambda(t)/\lambda(t+1))$ and our fits, where fit range is determined based on $\chi^2/d.f.$. The errors-bars of the final energy values correspond to statistical errors obtained using single-elimination jack-knife.

H. Scattering length

We determine the s-wave scattering length a_0 for $B_s\pi$ scattering from the ground state energy E_{gr}^{lat} on the lattice using Lüscher's relation [24, 25]

$$a_0^{B_s\pi} \equiv \lim_{p\to 0} \frac{1}{p\cot\delta(p)} = \frac{\sqrt{\pi}L}{2Z_{00}(1;(p_{gr}L/2\pi)^2)} \tag{12}$$

The momentum p_{gr} is obtained as discussed earlier in Subsection III C.

IV. RESULTS

We aim to determine the energies of eigenstates for the system with flavor $\bar{b}s\bar{d}u$, $J^P = 0^+$ and total momentum zero, and compare them to analytic predictions for the scenarios in the previous section.

As mentioned above, we present the final energies as $E = E_n^{lat} - E_{\overline{B}_s}^{lat} + E_{\overline{B}_s}^{exp}$. The upper pane of Figure 3 shows the results for the energy levels from correlated (full symbols) and uncorrelated (open symbols) fits to the t-dependence for the three lowest eigenstates for two choices of interpolator basis (A and B) and two set of gauge configurations ("all" and "all-4"). While there is a visible difference between those choices for single energy levels, the extracted value for the $B_s\pi$ scattering length displayed in the bottom pane of Figure 3 is largely independent of these choices. Furthermore none of these variations lead to an energy level in close vicinity to the X(5568).

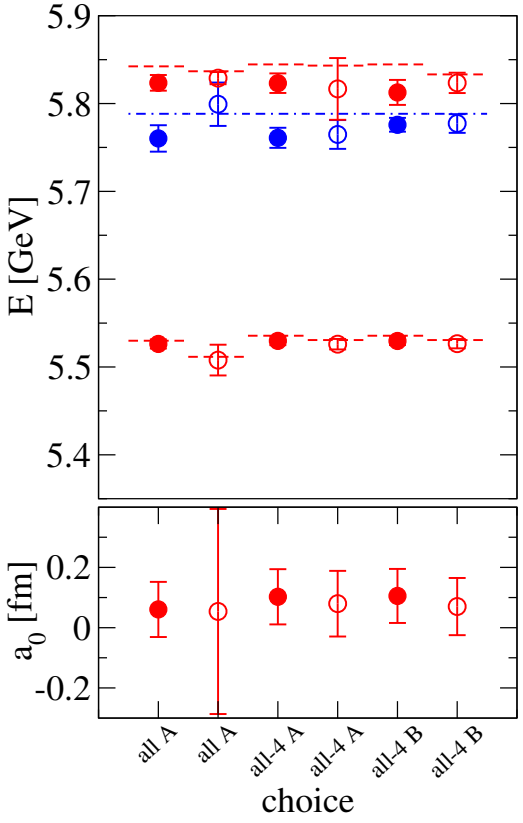

FIG. 3. The eigenenergies of the $\bar{b}s\bar{d}u$ system with $J^P = 0^+$ from a lattice simulation for various choices. The horizontal lines show energies of eigenstates $B_s(0)\pi^+(0)$, $B^+(0)\bar{K}^0(0)$ and $B_s(1)\pi^+(-1)$ in absence of interactions. The energies $E = E_n^{lat} - E_{\overline{B}_s}^{lat} + E_{\overline{B}_s}^{exp}$ are shown, where the spin-averaged ground state is set to its physical value. The sets with full symbols are from correlated fits to the t-dependence for $B_s\pi$ states while open symbols result from uncorrelated fits. Notation "all" refers to the full set of gauge configurations while "all-4" refers to the set with four (close to exceptional) gauge configurations removed. Set A is from interpolator basis $O_1^{B_s(0)\pi(0)}, O_1^{B_s(1)\pi(-1)}, O_1^{B(0)K(0)}$ while set B results from a larger basis $O_1^{B_s(0)\pi(0)}, O_{1,2}^{B_s(1)\pi(-1)}, O_{1,2}^{B(0)K(0)}$.

Our final results for the eigenenergies of the $\bar{b}s\bar{d}u$ system with $J^P = 0^+$ obtained from our simulation are presented in Figure 4a (correlated fit, choice "all A" from Figure 3). The circles in Figure 4b show the analytic predictions for the spectrum at our $L = 2.9$ fm if a resonance $X(5568)$ exists (same as in Figure 1). The analytic prediction based on $X(5568)$ renders an energy level near $E \simeq m_X \sim 5.57$ GeV, which is not observed in the ac-

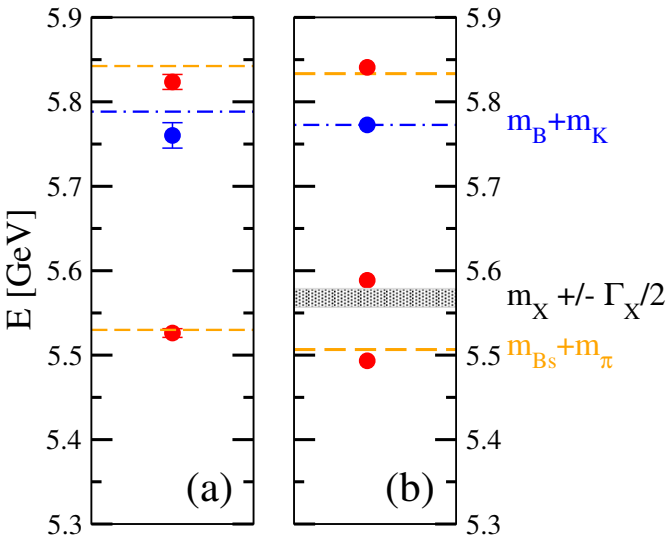

FIG. 4. (a) The eigenenergies of the $\bar{b}s\bar{d}u$ system with $J^P = 0^+$ from our lattice simulation and (b) an analytic prediction based on $X(5568)$, both at lattice size $L = 2.9$ fm. The horizontal lines show energies of eigenstates $B_s(0)\pi^+(0)$, $B^+(0)\bar{K}^0(0)$ and $B_s(1)\pi^+(-1)$ in absence of interactions; momenta in units of $2\pi/L$ are given in parenthesis. The pane (a) shows the energies $E = E_n^{lat} - E_{\overline{B_s}}^{lat} + E_{\overline{B_s}}^{exp}$ with the spin-averaged B_s ground state set to its experiment value. The pane (b) is based on the experimental mass of the $X(5568)$ [1], given by the grey band, and experimental masses other particles.

tual simulation (left figure). Results of our simulation therefore do not provide support for the existence of an $X(5568)$ resonance with $J^P = 0^+$ in $B_s\pi$ scattering. The scenario of $X(5568)$ as a deeply bound $B^+\bar{K}^0$ also would render an energy level near $E \simeq m_X$, so this scenario is also not supported by the simulation.

The spectrum from the simulation is closer to the non-interacting limit indicated by the horizontal lines in Figure 4, indicating a rather weak interaction. These lines show energies $m_{B_s} + m_\pi$, $m_B + m_K$ and $E_{B_s(1)} + E_{\pi(-1)}$ of the relevant two-meson states $B_s(0)\pi(0)$, $B^+(0)\bar{K}^0(0)$ and $B_s(1)\pi(-1)$ in absence of interactions: in pane (a) the lines show the sum of single-particle energies obtained from the simulation, while pane (b) is based on the experimental masses. The lowest and highest eigenstates $|n\rangle$ have large overlap $\langle O|n\rangle$ with the $O^{B_s\pi}$ interpolator (red) and the middle state has large overlap with the O^{BK} interpolator (blue), which confirms their identification.

The resulting $B_s\pi$ scattering length a_0 (cf. Section III H) is small and compatible with zero within errors, as displayed in Figure 3. Our result is compatible with $a_0^{D_s\pi} = -0.002(1)$ fm obtained for a similar channel $D_s\pi$ from their ground eigenstate [42]. Using the value from reference [42, 43] as an input, the Chiral perturbation theory (ChPT) [44] for $B_s\pi$ and Unitarized ChPT [45] for $D_s\pi$ also leads to a very small scattering length in agreement with our lattice result.

V. CONCLUSIONS

If the exotic state $X(5568) \to B_s\pi^+$ observed by D0 exists, it could be one of the easiest exotic candidates to establish on the lattice. The state $X(5568)$ with the most natural quantum number $J^P = 0^+$ would represent a resonance in elastic $B_s\pi^+$ scattering, significantly below the next relevant threshold $B^+\bar{K}^0$. We presented the first simulation of $B_s\pi^+$ scattering in the channel $J^P = 0^+$, aiming to search for possible exotic resonances close to the threshold. For completeness we took into account also the $B^+\bar{K}^0$ channel, which has a threshold 210 MeV above $X(5568)$. In a system with a resonance, Lüscher's formalism predicts an eigenstate with $E \simeq m_X$ if $X(5568)$ exists, while such an eigenstate is not found in our simulation. Our results therefore do not support the existence of $X(5568)$ with $J^P = 0^+$. Instead, the results appear closer to the limit where B_s and π do not interact significantly.

Node added: After this manuscript appeared as preprint, the analytic study [46] presented the finite-volume spectrum in this channel based on the Unitarized ChPT [45]. Their analytic conclusion agrees with our conclusion from the lattice simulation.

Acknowledgments

We thank the PACS-CS collaboration for providing the gauge configurations. S.P. thanks R. Lebed and M. Pappagallo for clarifications on the experimental result. D.M. would like to thank M. Hansen for useful discussions. This work is supported in part by the Slovenian Research Agency ARRS and by the Austrian Science Fund project FWF:I1313-N27. The calculations were performed on Fermilab USQCD clusters and on computing clusters at the University of Graz (NAWI Graz). We thank the Fermilab Lattice Collaboration for allowing us to calculate the observables at Fermilab using previously stored propagators.

[1] D0, V. M. Abazov *et al.*, Phys. Rev. Lett. **117**, 022003 (2016), [arXiv:1602.07588].

[2] LHCb, R. Aaij *et al.*, Phys. Rev. Lett. **117**, 152003 (2016), [arXiv:1608.00435].

[3] S. S. Agaev, K. Azizi and H. Sundu, Phys. Rev. D **93**, 074024 (2016), [arXiv:1602.08642].
[4] Z.-G. Wang, Commun. Theor. Phys. **66**, 335 (2016), [arXiv:1602.08711].
[5] W. Chen, H.-X. Chen, X. Liu, T. G. Steele and S.-L. Zhu, Phys. Rev. Lett. **117**, 022002 (2016), [arXiv:1602.08916].
[6] C.-J. Xiao and D.-Y. Chen, 1603.00228.
[7] S. S. Agaev, K. Azizi and H. Sundu, Eur. Phys. J. Plus **131**, 351 (2016), [arXiv:1603.02708].
[8] R. Albuquerque, S. Narison, A. Rabemananjara and D. Rabetiarivony, Int. J. Mod. Phys. **A31**, 1650093 (2016), [arXiv:1604.05566].
[9] T. J. Burns and E. S. Swanson, Phys. Lett. **B760**, 627 (2016), [arXiv:1603.04366].
[10] F.-K. Guo, U.-G. Meißner and B.-S. Zou, Commun. Theor. Phys. **65**, 593 (2016), [arXiv:1603.06316].
[11] W. Wang and R. Zhu, Chin. Phys. **C40**, 093101 (2016), [arXiv:1602.08806].
[12] Y.-R. Liu, X. Liu and S.-L. Zhu, Phys. Rev. D **93**, 074023 (2016), [arXiv:1603.01131].
[13] F. Stancu, J. Phys. **G43**, 105001 (2016), [arXiv:1603.03322].
[14] Q.-F. Lü and Y.-B. Dong, 1603.06417.
[15] X. Chen and J. Ping, Eur.Phys.J. **C76**, 351 (2016), [arXiv:1604.05651].
[16] A. Esposito, A. Pilloni and A. D. Polosa, Phys. Lett. **B758**, 292 (2016), [arXiv:1603.07667].
[17] M. Albaladejo, J. Nieves, E. Oset, Z.-F. Sun and X. Liu, Phys. Lett. **B757**, 515 (2016), [arXiv:1603.09230].
[18] X.-W. Kang and J. A. Oller, Phys. Rev. **D94**, 054010 (2016), [arXiv:1606.06665].
[19] J. J. Dudek, R. G. Edwards and C. E. Thomas, Phys. Rev. **D87**, 034505 (2013), [arXiv:1212.0830].
[20] C. Pelissier and A. Alexandru, Phys. Rev. D **87**, 014503 (2013), [arXiv:1211.0092].
[21] C. B. Lang, D. Mohler, S. Prelovsek and M. Vidmar, Phys. Rev. D **84**, 054503 (2011), [arXiv:1105.5636].
[22] S. Prelovsek, L. Leskovec, C. B. Lang and D. Mohler, Phys. Rev. D **88**, 054508 (2013), [arXiv:1307.0736].
[23] D. Mohler, S. Prelovsek and R. M. Woloshyn, Phys. Rev. D **87**, 034501 (2013), [arXiv:1208.4059].
[24] M. Lüscher, Nucl. Phys. B **354**, 531 (1991).
[25] M. Lüscher, Nucl. Phys. B **364**, 237 (1991).
[26] S. Aoki *et al.*, Phys. Rev. D **79**, 034503 (2009), [arXiv:0807.1661].
[27] C. B. Lang, L. Leskovec, D. Mohler, S. Prelovsek and R. M. Woloshyn, Phys. Rev. D **90**, 034510 (2014), [arXiv:1403.8103].
[28] A. X. El-Khadra, A. S. Kronfeld and P. B. Mackenzie, Phys. Rev. D **55**, 3933 (1997), [arXiv:hep-lat/9604004].
[29] M. B. Oktay and A. S. Kronfeld, Phys. Rev. D **78**, 014504 (2008), [arXiv:0803.0523].
[30] C. B. Lang, D. Mohler, S. Prelovsek and R. M. Woloshyn, Phys. Lett. **B750**, 17 (2015), [arXiv:1501.01646].
[31] A. S. Kronfeld, Phys. Rev. D **62**, 014505 (2000), [arXiv:hep-lat/0002008].
[32] M. Padmanath, C. B. Lang and S. Prelovsek, Phys. Rev. **D92**, 034501 (2015), [arXiv:1503.03257].
[33] S. J. Brodsky, D. S. Hwang and R. F. Lebed, Phys. Rev. Lett. **113**, 112001 (2014), [arXiv:1406.7281].
[34] S. Prelovsek, C. B. Lang, L. Leskovec and D. Mohler, Phys. Rev. **D91**, 014504 (2015), [arXiv:1405.7623].
[35] C. Morningstar *et al.*, Phys. Rev. D **83**, 114505 (2011), [arXiv:1104.3870].
[36] Hadron Spectrum Collaboration, M. Peardon *et al.*, Phys. Rev. D **80**, 054506 (2009), [arXiv:0905.2160].
[37] C. Michael, Nucl. Phys. B **259**, 58 (1985).
[38] M. Lüscher, Commun. Math. Phys. **104**, 177 (1986).
[39] M. Lüscher and U. Wolff, Nucl. Phys. B **339**, 222 (1990).
[40] B. Blossier, M. Della-Morte, G. von Hippel, T. Mendes and R. Sommer, JHEP **0904**, 094 (2009), [arXiv:0902.1265].
[41] S. Prelovsek *et al.*, Phys. Rev. D **82**, 094507 (2010), [arXiv:1005.0948].
[42] L. Liu, K. Orginos, F.-K. Guo, C. Hanhart and U.-G. Meißner, Phys. Rev. D **87**, 014508 (2013), [arXiv:1208.4535].
[43] L. Liu, H.-W. Lin and K. Orginos, PoS **LATTICE2008**, 112 (2008), [arXiv:0810.5412].
[44] Y.-R. Liu, X. Liu and S.-L. Zhu, Phys. Rev. **D79**, 094026 (2009), [arXiv:0904.1770].
[45] M. Altenbuchinger, L. S. Geng and W. Weise, Phys. Rev. D **89**, 014026 (2014), [arXiv:1309.4743].
[46] J.-X. Lu, X.-L. Ren and L.-S. Geng, 1607.06327.